nature protocols

https://doi.org/10.1038/s41596-024-01080-1

Protocol

Check for updates

A multiwell plate approach to increase the sample throughput during tissue clearing

Fumito Akiyama[1,2,6], Katsuhiko Matsumoto[1,3,6], Katsunari Yamashita[1,4], Akio Oishi[2], Takashi Kitaoka[2] & Hiroki R. Ueda[1,3,4,5]

Abstract

Tissue clearing, coupled with immunostaining, enables the transition from two-dimensional to three-dimensional pathology and has the potential to substantially improve data quality for biomedical diagnostics. Nevertheless, the workflows are limited by the complex sample processing protocols. Approaches for the parallel processing of samples, to include tissue clearing, immunostaining, imaging and analysis can increase three-dimensional pathology throughput. Here we detail a step-by-step approach that combines a tissue clearing device with a six-well multiwell plate to increase the throughput compared with methods using conventional clearing protocols. The six-well multiplate allows for parallel tissue clearing of multiple samples and is compatible with passive tissue clearing methods including Clear, Unobstructed Brain/Body Imaging Cocktails and Computational (CUBIC) analysis. In addition, gel embedding is performed without moving the samples from the wells, and a series of steps such as imaging with a high-speed light-sheet microscope and analysis in the cloud can be performed. Although this procedure slightly extends the overall time required for preparing and analyzing a single sample, it reduces the effort required at each step, such as reagent exchange and gel embedding, which results in an overall reduction in hands-on time due to the parallel sample processing. We describe a series of whole-organ analyses, including high-throughput tissue clearing, staining, gel embedding, imaging and data analysis in the cloud, as a useful platform for cellular biology and pathology. The total process varies depending on the presence or absence of immunostaining, but for some six-well plates, the tissue clearing process, imaging and data analysis can be completed within 10 d.

Key points

- In this modified tissue clearing protocol, a multiwell plate is combined with a tissue clearing insert device to enable the parallelization of the tissue clearing process.
- This procedure streamlines the complex task of reagent exchange during the clearing process.

Key references

Tainaka, K. et al. *Cell Rep.* **24**, 2196–2210.e9 (2018): https://doi.org/10.1016/j.celrep.2018.07.056

Susaki, E. A. et al. *Nat. Commun.* **11**, 1982 (2020): https://doi.org/10.1038/s41467-020-15906-5

Mano, T. et al. *Cell Rep. Methods* **1**, 100038 (2021): https://doi.org/10.1016/j.crmeth.2021.100038

[1]Laboratory for Synthetic Biology, Center for Biosystems Dynamics Research, RIKEN, Suita, Japan. [2]Department of Ophthalmology and Visual Sciences, Graduate School of Biomedical Sciences, Nagasaki University, Nagasaki, Japan. [3]Department of Systems Pharmacology, University of Tokyo, Tokyo, Japan. [4]Department of Systems Biology, Graduate School of Medicine, Osaka University, Suita, Japan. [5]Institute of Life Science, Kurume University, Kurume, Japan. [6]These authors contributed equally: Fumito Akiyama, Katsuhiko Matsumoto. e-mail: uedah-tky@umin.ac.jp

Introduction

Tissue clearing methods

The tissue clearing technique has been developed over 100 years. Weiteres Lundvall in Sweden and Walter Spalteholz in Germany were the pioneers who first achieved tissue clearing using hydrophobic reagents[1,2]. In 1995, Valery Tuchin in Russia developed tissue clearing reagents using hydrophilic chemicals (X-ray contrast agents, alcohols such as glycerol, sugars such as glucose, and dimethylsulfoxide)[3,4]. In 2007, Hans-Ulrich Dodt and colleagues cleared a whole fly, a mouse whole brain and a mouse embryo using the organic-solvent-based clearing method and imaged the whole organ/body in combination with a light-sheet microscope and opened the door for whole-organ analysis[5,6]. In 2013, Chung, Deisseroth and colleagues developed a hydrogel embedding tissue clearing technique called CLARITY[7]. This decade has seen the development of many tissue clearing methods that are developed and applied to various fields of biological research[5–51].

Tissue clearing techniques are broadly categorized into three main methods: hydrophobic clearing, hydrophilic clearing and hydrogel embedding, and each method has its distinctive features. Hydrophobic clearing techniques such as 3Disco and BABB provide rapid clearing and high transparency[17,18,21–23,52]. Hydrophilic tissue clearing methods use relatively safe reagents and maintaining the fluorescent proteins[8–11,35,46]. Hydrogel-embedded tissue clearing, such as CLARITY, maintains fluorescent proteins and provides high transparency[7,20,34]. It is crucial to carefully select a method according to the specific requirements of the experiments, considering the unique characteristics of each method.

Clear, Unobstructed Brain/Body Imaging Cocktails and Computational (CUBIC) analysis is a tissue clearing technique that uses hydrophilic reagents, enabling the clearing of most organs in mice while maintaining the fluorescence of fluorescent proteins[10,11,46]. However, it should be noted that its disadvantages include the longer time required for clearing and the need for frequent reagent changes. CUBIC tissue clearing enables the highly efficient clearing of biological samples by delipidation and adjusting the refractive index (RI) with multiple reagents. The combination of tissue clearing and three-dimensional (3D) immunostaining is expected to advance biological research at the whole-organ/body scale and in 3D pathology, but these studies would benefit from a high-throughput tissue clearing protocol. Passive tissue clearing methods, including CUBIC, require more time for processing, yet can accommodate parallel processing. However, the reagents need to be changed frequently, which is time consuming and may damage the sample during the reagent change process. Therefore, we have developed a protocol that combines novel tissue clearing insert devices with six-well multiwell plates to increase the throughput of tissue clearing and minimize sample damage by reducing contact with the sample during the tissue clearing process. The combination of a widely used multiwell plate and the tissue clearing insert device that can be made with a 3D printer, rather than a proprietary device, facilitates implementation. Hydrophilic reagents such as CUBIC can be used without affecting the plastic plates. This protocol allows for parallel tissue clearing for not only mouse brains, but also other organs.

Volumetric imaging and data analysis for whole organs

Several methods are available for 3D imaging at the whole mouse organ scale. The combination of light-sheet microscopy and tissue clearing techniques has been reported in many studies[5,12,13,29,47,53–69]. Confocal microscopy and multiphoton fluorescence microscopy are also used for detailed volume imaging of smaller areas. Here, we constructed a light-sheet microscope with variable magnification (0.4–4×) and equipped with the high-speed imaging technique MOVIE-scan for fast whole-organ-scale 3D imaging compatible with high-throughput tissue clearing methods[47]. Although several commercially available light-sheet microscopies are available and they can be used, care should be taken regarding throughput, resolution and the sample size that can be imaged. If the sample holder of the microscope is large enough to place this device, this protocol can be used without modification. If the sample holder is smaller,

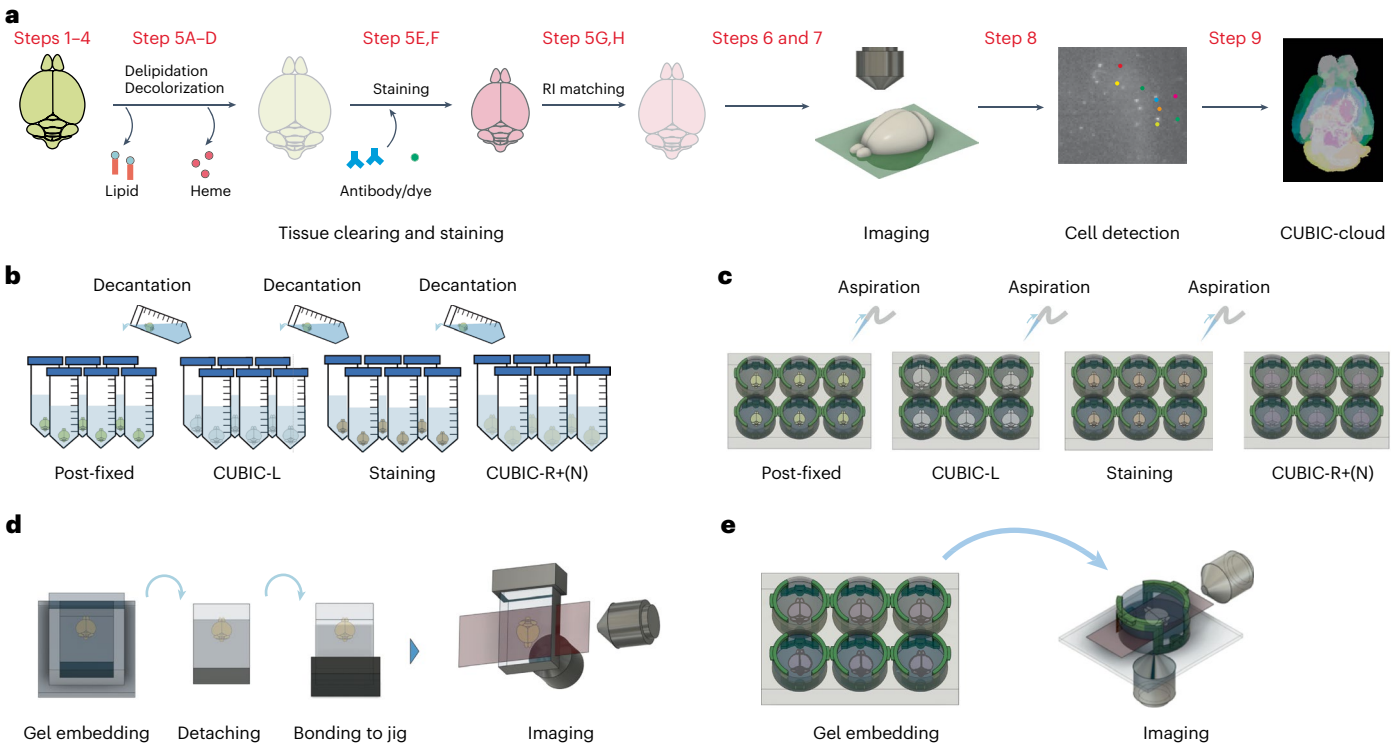

Fig. 1 | Workflow of high-throughput CUBIC pipeline and comparison with the conventional method. a, The overall workflow of the CUBIC pipeline. Each step includes delipidation, staining, RI matching, imaging, and data analysis using CUBIC-Cloud (Steps 1–9). **b**, A conventional tissue clearing protocol using conical tubes. **c**, A high-throughput tissue clearing protocol using six-well multiwell plates and tissue clearing insert devices. **d**, The procedure for gel embedding and imaging of samples using the conventional method. This requires a proprietary gel mold and fixation to a jig for imaging. **e**, Gel embedding of samples using the tissue clearing insert device in the six-well multiwell plate. This can be directly transferred to imaging.

the cleared sample can be removed from the six-well plate and mounted for each microscope in the recommended manner, and imaging can be performed.

Experimental design

Overview of the high-throughput CUBIC pipeline

Whole-organ-scale analysis using the basic CUBIC pipeline was constructed with three steps: tissue clearing, imaging and data analysis. The tissue clearing step includes delipidation and decolorization with CUBIC-L (Step 5A–C), staining with CUBIC-HistVIsion (CUBIC-HV) (Step 5E,F) and RI matching with CUBIC-R+(N) (Step 5G,H). The cleared organs are imaged using a light-sheet microscope (Step 8) and the cells of interest are detected from volumetric images and analyzed on the CUBIC-Cloud (Fig. 1a) (Step 9). Conventional CUBIC tissue clearing using conical tubes requires a lot of labor to clear many samples, but this high-throughput tissue clearing protocol using a tissue clearing insert device with an aspirator and dispenser facilitates solution exchange without direct contact and reduces the risk of sample damage (Fig. 1b,c). Regarding the time required for changing the solution, when using tubes, it takes ~30 s per sample, but when using a six-well plate, it takes ~40 s per plate (7 s per sample). The difference in time, especially when handling a large number of samples on the order of 100 samples, is not only significant, but the labor required to open and close the tubes (weak closure can cause leakage) is also considerable. When using tubes, there was a risk of samples falling or getting damaged by spoons during reagent exchange. In particular, samples after CUBIC-L treatment are very soft and fragile, so a small problem can easily cause major damage. Undamaged cleared tissues are appropriate for accurate experiments as any damage to the sample may affect quantitative analysis and the accuracy of mapping to the atlas. Moreover, the conventional method requires embedding the sample in three layers of agarose and complicated steps

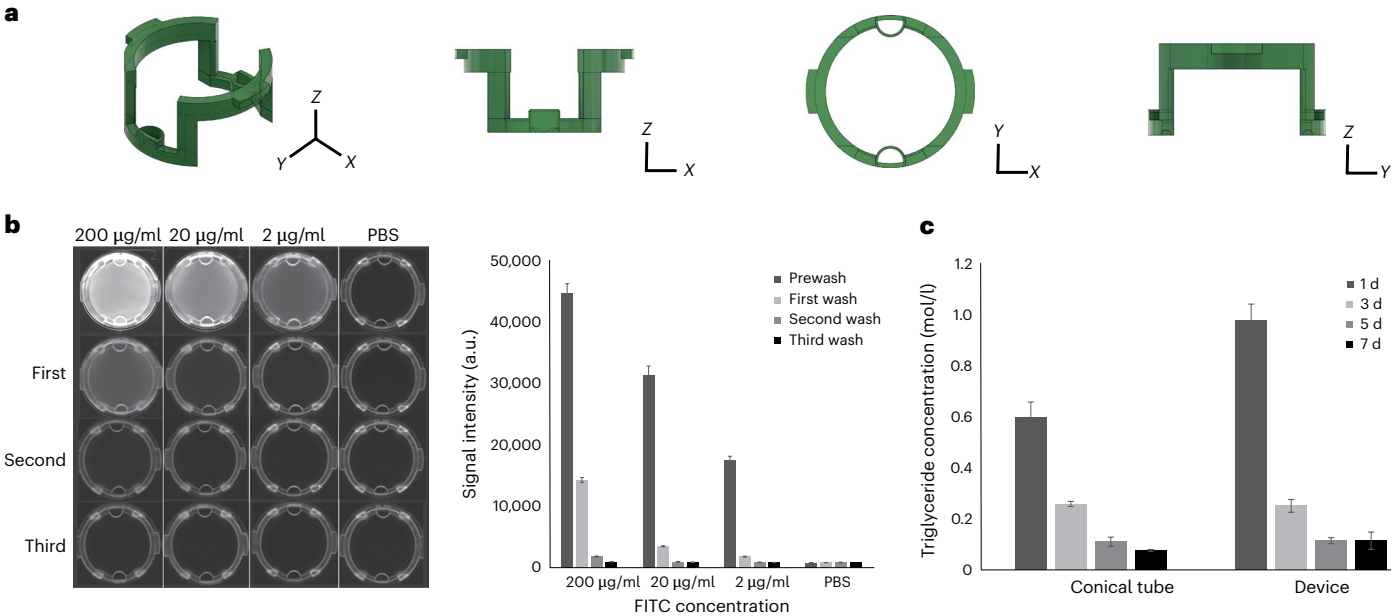

Fig. 2 | Design of tissue clearing insert device and its performance. a, Three-dimensional CAD images of the tissue clearing insert device. **b**, Fluorescence images (left) and bar graph (right) for quantification of the remaining FITC fluorescence intensity after each of the three solution changes. **c**, Quantification of the eluted triglyceride concentration in CUBIC-L solution after the delipidation step with conical tubes and devices. The *y* axis indicates the triglyceride concentration measured using the EnzyChrom Triglyceride Assay Kit. The error bars in **b** (right graph) and **c** are the standard deviation.

including fixation are required for microscopic imaging, but this tissue clearing insert device simplifies the process because the sample can be embedded in the well with device and imaged directly with a light-sheet microscope or other microscopes (Fig. 1d,e).

Design of the tissue clearing insert device

The tissue clearing insert device for the six-well multiwell plate was designed using 3D computer aided design (CAD) software (Autodesk, Fusion360) (Fig. 2a and Supplementary Data 1). The size of the device was designed to fit tightly within the wells. If it is too small, it rotates in the wells and becomes unstable. We examined the 3D printing method and resin, and selected a light-curing 3D printer that can create finer structures and a resin with moderate elasticity. The well size may require fine tuning as it may vary slightly from manufacturer to manufacturer. A drainage space was designed to avoid any damage to the sample from the aspirator during the process of changing solutions. The shape was designed to allow the device to be embedded in the well and the gel to be easily pulled out of the well and not interfere with the light sheet when acquired by light-sheet microscopy. First, the fluorescence intensity of FITC was measured to verify the efficiency of reagent exchange when the aspirator and dispenser were used. FITC and PBS at concentrations of 200 µg/ml, 20 µg/ml and 2 µg/ml were filled into the wells individually. After reagent removing using an aspirator, the plates were washed three times with PBS and the changes of fluorescence intensity were measured. Fluorescence intensities were measured by the gel imaging system, and the average value of the center region ($N = 3$) was calculated using ImageJ. As a result, even with high concentrations of FITC, the fluorescence intensity decreased to the same level as PBS after three washes, verifying that almost all compounds are washed out after three washes (Fig. 2b). Next, we verified that the limited volume of solution in the six-well plate was enough to delipidate. CUBIC-L (1/2 CUBIC-L on day 1) was added to a conical tube and a six-well plate in volumes of 10 ml and 7.5 ml, respectively, and fixed mouse brains were treated for 7 d and the triglyceride concentration in CUBIC-L was quantified at each reagent exchanges. Quantification was performed using the EnzyChrom Triglyceride Assay kit (BioAssay Systems). Fluorescence intensity was measured and the triglyceride concentration in the solution was determined by standardization against the control. As a result, almost the same delipidation efficiency was observed. (Fig. 2c).

Advantages of the high-throughput tissue clearing protocol

A liquid crystal display illumination type of light-curing 3D printer was selected to fabricate the tissue clearing insert devices (Fig. 3a). Owing to its ability to produce more detail than filament-based 3D printers, it is suitable for the fabrication of curved surfaces. In addition, it is possible to fabricate at relatively high speeds. Flexible resins are used, which fit in the wells and prevent rotation of the device and minimize damage that may occur to the sample during the clearing process. During the CUBIC tissue clearing process, the sample is expanded and softened so that it increases the risk of damages. In this protocol, reagents are exchanged from the drain space, decreasing the risk for contact to the sample and reducing the risk of damage. In addition, the protocol using conical tubes requires a lot of time and effort to open and close the tube lids for handling a large number of samples, but in this protocol it is easy to open and close the lids and requires fewer times to it, reducing the burden on the researcher (Fig. 3b). As a result, the time required was reduced by ~4–5 times. When many samples are processed for tissue clearing simultaneously in the incubator, this protocol saves space compared with the previous protocol. This allows more samples to be processed in the same space,

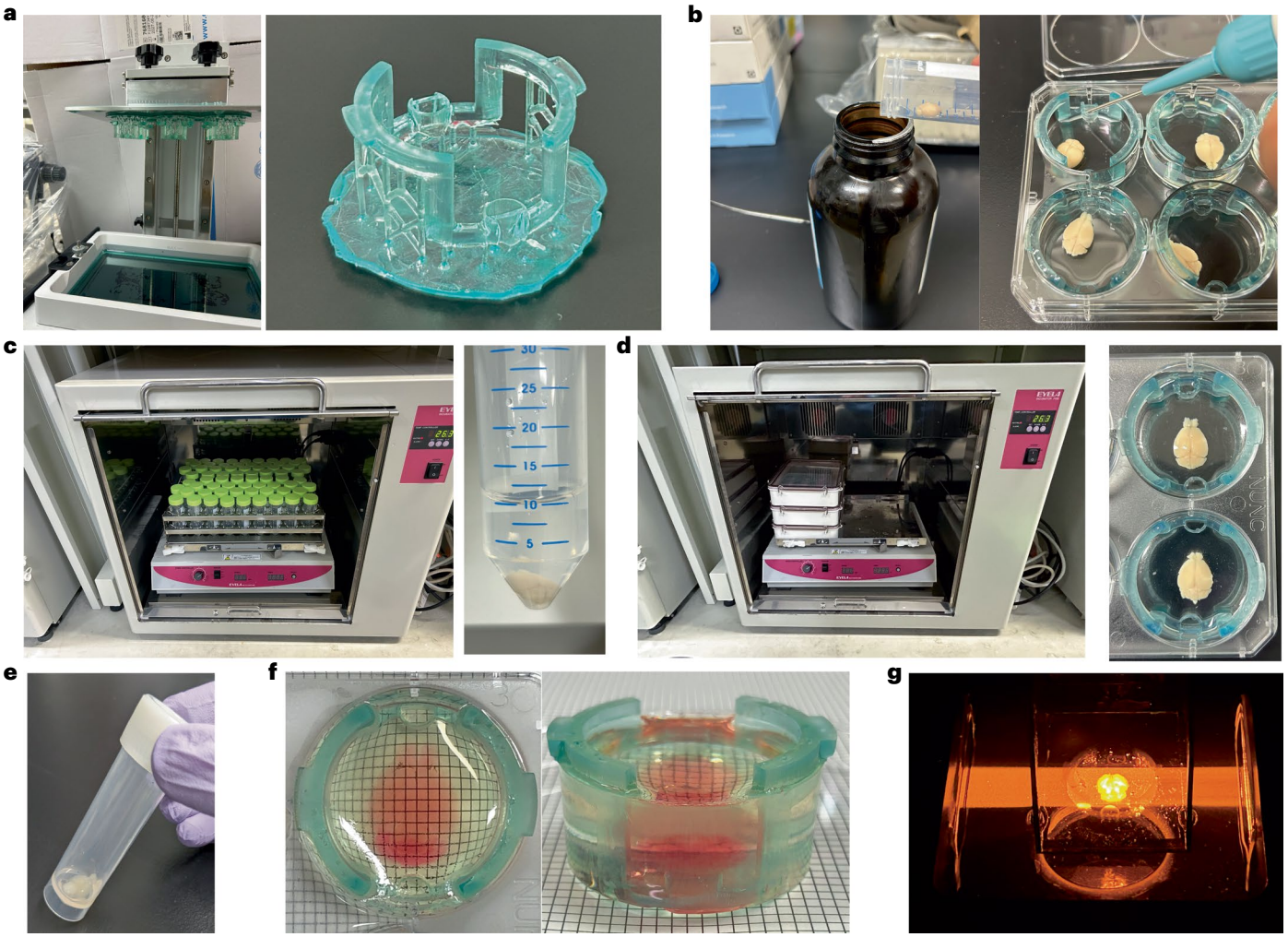

Fig. 3 | Advantages of the tissue clearing insert device. a, The process of creating the tissue clearing insert device using a 3D printer. **b**, The reagent exchange step using a conical tube and tissue clearing insert device. **c**, Photo showing the incubation of 84 samples prepared using the conventional tissue clearing method using conical tubes. **d**, Photo showing the incubation of 84 samples prepared using the high-throughput tissue clearing method. We typically seal plates in a container to avoid evaporation using containers that can fit up to a maximum of four plates. **e**, Photo showing the immunostaining step using a immunostaining tube. **f**, Gel embedding with the tissue clearing insert device (Steps 6 and 7). The gel surface is smooth and the sample is not exposed on the gel surface. Grid size, 2 mm. **g**, Imaging with light-sheet microscopy of a cleared mouse brain embedded with the tissue clearing insert device (Step 8).

resulting in a higher throughput of the tissue clearing process (Fig. 3c,d, 84 samples each). To image cleared organs, we recommend embedding organs in a gel made of CUBIC-R+(N) and 2% agarose (Step 6). While imaging without gel embedding is possible, light scattering may occur on the sample surface and it becomes artifact such as the stripe; therefore, embedding in gel is necessary to obtain higher-precision images. In this protocol, gel embedding can be performed with the sample and tissue clearing insertion device still in the wells. By filling the wells with agarose–CUBIC-R+(N) in two steps, the samples can be embedded without uncovering the surface of the gel. The sides of the gel are smoothly curved around the wells. Even if the sides of the gel are curved, this does not affect imaging by light-sheet microscopy and does not cause distortion of the light sheet by carefully matching the RI of the immersion oil with agarose–CUBIC-R+(N) gel. Our custom-made light-sheet microscope places the objective lens for observation under the sample, and the bottom of the gel is flat and smooth, which allows for clear imaging (Fig. 3e,f).

Overview of the high-throughput tissue clearing protocol

After perfusion fixation with 4% paraformaldehyde (PFA) and dissection, organs are put into the six-well plate with the tissue clearing insert device and additional fixation was performed with 4% PFA at 4 °C for overnight (Steps 2–3). Subsequently, samples are washed with PBS at least three times (Step 4). For the initial delipidation, samples are incubated in 50% CUBIC-L for 1 d (Step 5A) then incubated in 100% CUBIC-L for 6 d to complete delipidation (CUBIC-L was refreshed every 2 d; Step 5B). The delipidation period may need to be adjusted depending on the sample size. After delipidation, samples are washed with PBS at least three times (Step 5C). RI matching was also performed on the plate (Step 5G,H). This protocol was applied not only to the brain, but also to other organs of the mouse. (Fig. 4a,c,d and Supplementary Fig. 1). To clear melanin pigment-rich organs such as the eyes, an additional step of decolorization with hydrogen peroxide is added (Fig. 4b,e) (Step 5D). When performing the nuclear staining, the samples are treated with the nuclear staining buffer, followed by a 3 d staining period with the specified amount of nuclear staining reagent in the well (propidium iodide (PI), RedDot 2 (RD2) and SYTOX-G) (Step 5E). When performing immunostaining, it is recommended that the conventional CUBIC-HV protocol is followed to minimize the amount of antibody. The immunostaining step requires carefully transferring each sample into a conical tube containing a staining buffer with antibodies (Fig. 3e). The samples are then gently shaken using the same shaker utilized for the CUBIC-L treatment. The immunostaining step requires transferring the sample into a conical tube (Fig. 3e). After the staining is completed, samples are returned to the plate and performed following steps such as wash and post-fixation on the plate. For demonstration, we stained mouse brain and other organs using some antibodies (anti-NeuN, anti-alpha-SMA and anti-CD31; Supplementary Figs. 3 and 4). Antibodies that have already reported to be compatible with CUBIC-HV can be used in this protocol[48]. We also performed other passive tissue clearing methods PACT and Sca*l*eS using this tissue clearing insert device for the whole mouse brain and 2-mm-thick slices and clearing were achieved (Supplementary Fig. 2).

Imaging by light-sheet microscopy

Volumetric imaging of cleared organs can be performed by light-sheet microscopy. The light-sheet microscope used here was constructed (see 'Equipment setup' section for details). For imaging of cleared organs, gel embedding with agarose–CUBIC-R+(N) is recommended to minimize light scattering and to reduce artifacts such as stripes (Steps 6 and 7). The gel-embedded tissue clearing insert device can be placed directly on the sample holder. No special fixation such as bonding or screwing is required. Even samples that are not gel embedded can be observed simply by placing on the sample holder. Light-sheet illumination is performed from either the left or right side of the sample and observed from bottom of the sample. *Z*-stack imaging is performed by moving the sample either from top to bottom or bottom to top with the MOVIE-scan method. Due to the narrow focus length of the light sheet compared with the field of view of the objective lens, the sample is moved in the *x*-direction to capture columnar

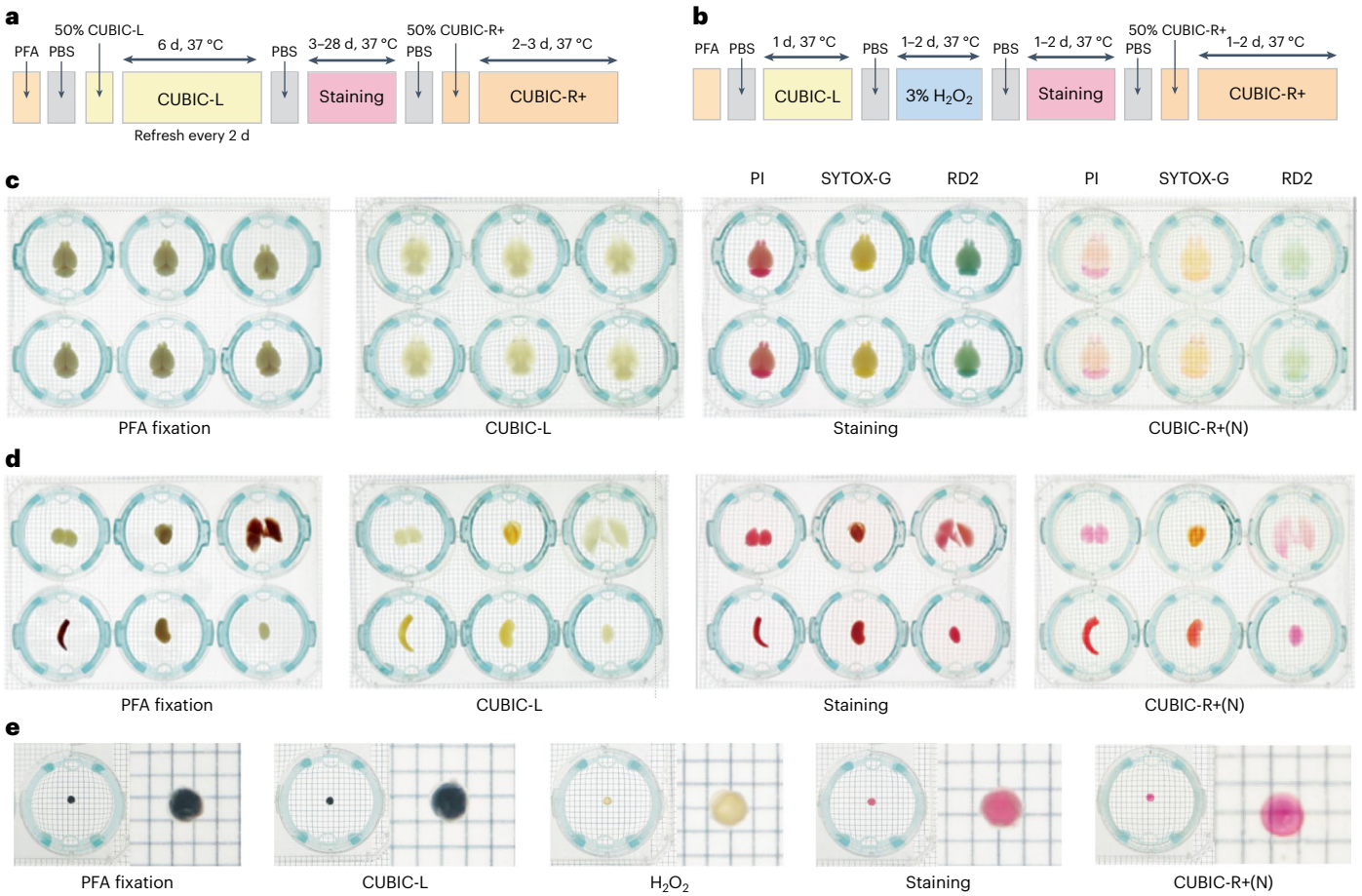

Fig. 4 | Tissue clearing protocols and clearing steps for mouse organs using high-throughput tissue clearing protocol. a, Tissue clearing and staining protocol for mouse brain and other mouse organs. **b**, Tissue clearing, decolorization and staining protocol for mouse eyes. **c**, Pictures of mouse brains after PFA fixation, delipidation with CUBIC-L, nuclear staining and RI matching with CUBIC-R+(N). Mouse brains were nuclear stained with PI, SYTOX-G and RD2, respectively (Steps 1–5). Grid size, 2 mm. **d**, Pictures of mouse organs (salivary gland, heart, lung, spleen, kidney and testis) after PFA fixation, delipidation with CUBIC-L, nuclear staining and RI matching with CUBIC-R+(N) (Steps 1–5). Grid size, 2 mm. **e**, Pictures of a mouse eye after PFA fixation, delipidation with CUBIC-L, decolorization with H_2O_2, nuclear staining and RI matching with CUBIC-R+(N) (Steps 1–5). Grid size, 2 mm.

images, which are then reconstructed entire images to achieve high *z*-resolution images across the entire sample. The number of columns taken was set to be even to switch the left and right illumination in the center of the sample, and ~16 tiles were taken for a mouse brain with 10 µm voxels (Step 8). Although a commercially available light-sheet microscope can be used, but the mounting method needs to be modified depending on the imageable sample size and imaging direction. For example, UltraMicroscope Blaze (Miltenyi Biotec) and Bruker Luxend light sheet microscope can be used without additional jigs, but note that Lightsheet7 (Zeiss) requires a jig to suspend the sample. In addition, consideration of imaging speed is necessary to using this high-throughput protocol.

Volumetric imaging using structured illumination microscopy

Cleared organs can be imaged with structured illumination microscopy (Keyence, BZ-X810). The cleared samples are embedded in gel and imaged from below while still in the multiwell plate. Since the plate is made of plastic, direct imaging may result in lower resolution. In such cases, increasing the resolution is possible by cutting out the gel and transferring it to a glass-bottom dish for imaging. However, regardless of the approach applied, deep imaging is more

difficult than with light-sheet microscopy. The microscope is useful for screening for thin or small samples in 3D, as it can capture images as thick as ~2 mm, is easy to set up and can easily capture images of multiple samples. Supplementary Fig. 3 shows volumetric images from cross-sections of immunostained mouse organs cut approximately in the center and imaged from the cut surface.

Data analysis using CUBIC-Cloud

Various methods and tools exist for extracting the target of interest from 3D images and they are applied for cleared organs[11,24,47,50,55,70,71]. Here, we describe a cell detection method that uses both GPU (graphics processing unit) and CPU (central processing unit) to identify point-shape signals (cells) from 3D images and data analysis using CUBIC-Atlas, which is a whole-brain all-cell atlas. At first, the ideal target point images (5 × 5 × 5 voxels) are calculated as it would be observed under a microscope. A point with the twice resolution of the actual image is created on the center of 11 × 11 × 11 voxels, and this point is moved one pixel in each of the *xyz* directions (27 variations in total). Gaussian filters are then applied to each image with multiple sigma values, which are subsequently scaled back to the original magnification (5 × 5 × 5 voxels). The sigma values are adjusted depend on the magnification and resolution. Next, a 3D maximum filter is used to detect 3D peaks in the image as cell candidates. The kernel size is set to a size corresponding to a cell (3 voxels in this case). Each cell candidate is normalized by the maximum and minimum values within a Manhattan distance of 2, and the similarity to the ideal cell image is calculated. The similarity is defined here as the sum of the difference between the values of each voxel (Step 9B). Peaks with values lower than a threshold are determined to be cells and their coordinates and intensities are output to a CSV file. Note that the distance to the point shape is used as the threshold value here and the closer to the point shape, the smaller the value. These CSV file and structural image file of cell nuclei or autofluorescence (resized to 50 µm in multi-tiff format) is uploaded to CUBIC-Cloud. Uploading these files will result in the mapping of cell coordinates on the CUBIC-Atlas on the cloud server, along with the region names of all cells, which are then converted to coordinates on CUBIC-Atlas. This mapping of cell coordinates enables comparative analysis between samples, and statistical analysis and visualization by each region and spatial coordinates are performed on CUBIC-Cloud (Fig. 5a and Step 9b,c).

To demonstrate the analysis using CUBIC-Cloud, we prepared schizophrenia mice model by administering MK-801 (Step 1), which is a noncompetitive antagonist of the *N*-methyl-D-aspartate (NMDA) receptor and stained with anti-c-Fos antibody. In addition, haloperidol was administered after MK-801 administration, and changes in neuronal activity were examined. Haloperidol or saline treated mice were also prepared as controls. Parvalbumin (PV) neurons, which are inhibitory neurons, were also stained with an anti-PV antibody and the c-Fos and PV signals were compared. Spatial heat maps (grid size of 200 µm, radius of 500 µm) and regional heat maps of c-Fos-positive cell numbers for four groups (each $n = 3$) are shown in Fig. 5b and Supplementary Figs. 6, 7 and 8. The resolution of the spatial heat maps, slice direction (sagittal, coronal, horizontal) and region of depicted brain are selectable on the CUBIC-Cloud. Spatial *P* value maps showing significantly changed regions in each sample group indicate an increase in the number of c-Fos-positive cells in the striatum in the haloperidol group and a widespread increase in MK-801 (Fig. 5c and Supplementary Figs. 9 and 10). However, the administration of haloperidol reduced the number of c-Fos-positive cells in the cortex. Comparing c-Fos and PV double-positive cells, an increase in double-positive cells was observed in parts of the cortex. As shown above, using CUBIC-Cloud enables easy mapping to the CUBIC-Atlas, statistical analysis calculations and visualization of the 3D point image. In addition, cell coordinates and regional information after mapping to the CUBIC-Atlas can be downloaded in CSV format, allowing detailed analysis by the user.

Expertise needed to implement the protocol

This procedure requires experience with mouse dissection, microscopy and data analysis. To implement these protocols in the most effective manner, experience with tissue clearing

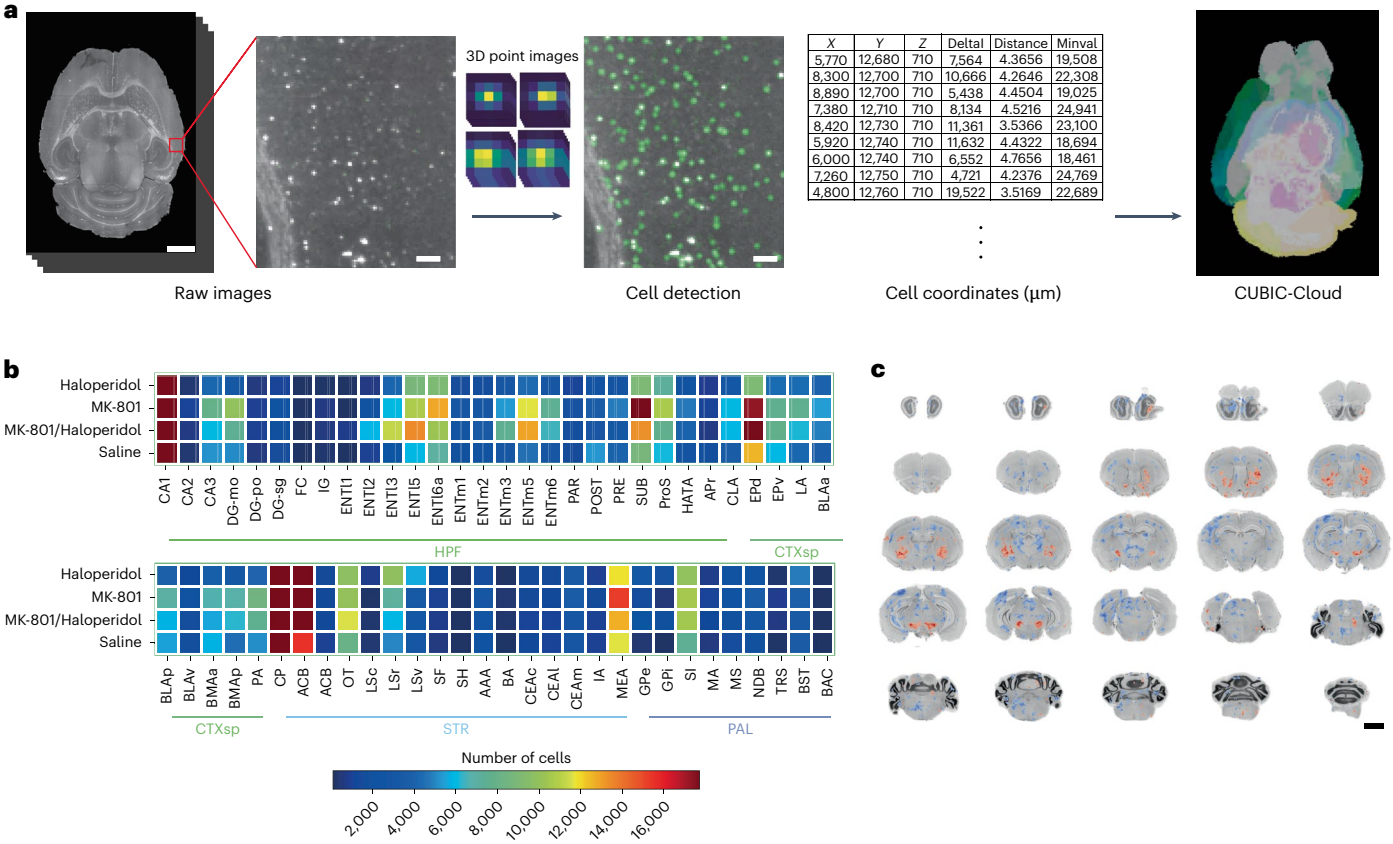

Fig. 5 | Cell detection and data analysis using CUBIC-Cloud. a, The workflow for cell detection and CUBIC-Cloud analysis for all brain regions. Scale bars, 3 mm (left) and 200 μm (middle and right). **b**, Heat map of the number of c-Fos-positive cells in some brain regions. The figure was generated by CUBIC-Cloud. All regions of the brain are shown in Supplementary Fig. 8. **c**, A spatial *P* value map generated by CUBIC-Cloud of the number of c-Fos-positive cells in a mouse brain administered with MK-801 before and after haloperidol administration. Grid size, 200 μm; radius, 500 μm; and scale bar, 5 mm. Deltal, the minimum difference between the peak and the minimum value in the 22 neighborhood; Minval, minimum value; HPF, hippocampal formation; CTXsp, cortical subplate; STR, striatum; PAL, pallidum.

methods and construction of microscopy, knowledge of programming languages such as Python or C++, and experience with image analysis and hardware control using these methods are required. When using a commercially available light-sheet microscope, device design expertise using 3D-CAD is required, as the device shape needs to be adjusted according to the illumination and observation direction of the microscope.

Limitations of the current CUBIC pipeline

Tissue clearing protocols based on CUBIC including minor modification methods have been reported and applied to various research fields. As improvements in tissue clearing technology has led to improvements in 3D immunostaining technology, it is now possible to perform immunostaining on various mouse organs. Recently, in combination with hydrogen peroxide, it has become possible to decolorize and clarify the pigment of the eye. However, tissue clearing and 3D staining of large organs requires a lot of time so further technological development is needed to use them in research. Regarding volumetric imaging, light-sheet microscopes are widely used for imaging transparent organs, but the equipment is costly and not easy to install. In addition, it is difficult to observe microscopic structures such as synapses. High-resolution volumetric imaging of whole organs requires the design of the lens with high numerical aperture (NA) and long working distance, the development of high-speed imaging methods and technologies for processing and storing or compressing for vast amounts of data.

Materials

- All materials are available from general vendors
  ▲ **CAUTION** For the laser, safety standards are established (IEC 60825-1) and lasers are classified according to their output. Appropriate labeling and other measures are required based on the class. Since laws may vary by country or region, please comply with the laws applicable to your respective area.

Reagents

- All reagents, including CUBIC reagents, can be purchased from common vendors
  ▲ **CAUTION** Each safety data sheet should be checked and stored and used in accordance with the Poisonous and Deleterious Substances Control Law and the Pollutant Release and Transfer Register (PRTR) laws for the respective region.

Animal samples

- We usually use C57BL/6J (CLEA) mice to prepare cleared organs
  ▲ **CAUTION** Animal experiments must be performed following governmental and institutional rules. All animal experiments and housing conditions in this report were authorized by the Animal Care and Use Committee of the RIKEN Institute and all animals were treated humanely along with the institutional guidelines for experiments using animals.

Perfusion, fixative and storage reagents

- PBS tablets, pH 7.4 (Takara, cat. no. T9181)
- Dulbecco's phosphate-buffered saline (Thermo Fisher, cat. no. 14190144)
- 1 mol/l HEPES buffer solution (Nacalai Tesque, cat. no. 17557-94)
- Sodium azide (Nacalai Tesque, cat. no. 31208-82)
  ▲ **CAUTION** Sodium azide is toxic. Avoid its inhalation and contact with the skin or the eyes.
- 4% PFA phosphate buffer solution (Wako, cat. no. 163-20145)
  ▲ **CAUTION** PFA is toxic. Perform all procedures in a fume hood. Avoid inhalation and exposure to the skin or the eyes.
- Formaldehyde solution (Nacalai Tesque, cat. no. 16222-65)
  ▲ **CAUTION** Formaldehyde is toxic. Perform all procedures in a fume hood. Avoid inhalation and exposure to the skin or the eyes.
- NaCl (Nacalai Tesque, cat. no. 31320-05 or 31319-45)

Tissue clearing and staining reagents

- Tissue clearing reagent CUBIC-L (for animals) (CUBICStars, cat. no. CSCR001)
  ▲ **CRITICAL** CUBIC-L can be prepared as described in 'Reagent setup', but a premixed and quality-controlled solution is also commercially available.
  ▲ **CAUTION** The patent for the CUBIC reagent is owned by RIKEN.
- Tissue clearing reagent CUBIC-R+(N) (for animals (CUBICStars, cat. no. CSCR002)
  ▲ **CRITICAL** Tissue clearing reagent CUBIC-R+(N) (for animals) can alternatively be prepared as described in 'Reagent setup'.
  ▲ **CAUTION** The patent for the CUBIC reagent is owned by RIKEN.
- *N*-Butyldiethanolamine (Tokyo Chemical Industry, cat. no. B0725)
- PEG mono-*p*-isooctylphenyl ether (Triton X-100; Nacalai Tesque, cat. no. 12967-45)
- 2,3-dimethyl-1-phenyl-5-pyrazolone (antipyrine; Tokyo Chemical Industry, cat. no. D1876)
- Nicotinamide (nicotinamide (N)) (Tokyo Chemical Industry, cat. no. N0078)
- CUBIC-HV1 3D nuclear staining kit (CUBICStars, cat. no. CSSR001)
- CUBIC-HV1 3D immunostaining kit (CUBICStars, cat. no. CSSR002)
- *N*,*N*,*N*′,*N*′-Tetrakis(2-hydroxypropyl)ethylenediamine (Quadrol; Tokyo Chemical Industry, cat. no. T0781)
- Hydrogen peroxide (H_2O_2, ~30%, Wako, cat. no. 7722-84-1)

- PI (Life Technologies, cat. no. P21493)
  ▲ **CAUTION** PI is light sensitive.
- RD2 (Biotium, cat. no. 40061)
  ▲ **CAUTION** RD2 is light sensitive.
- SYTOX green nucleic acid stain (SYTOX-G, Thermo Fisher, cat. no. 40061)
  ▲ **CAUTION** SYTOX-G is light sensitive.
- Anti-NeuN Antibody, clone A60 (NeuN, Merck, cat. no. MAB377, RRID:AB_2298772)
- Anti-c-Fos antibody (2H2) (c-Fos, Abcam, cat. no. ab208942, RRID:AB_2747772)
- Anti-Parvalbumin antibody (EPR13091) (PV, Abcam, cat. no. ab181086, RRID:AB_2924658)
- Anti-Actin, α-smooth muscle antibody, Mouse monoclonal (αSMA, Sigma-Aldrich, cat. no. A5228, RRID:AB_262054)
- CD31/PECAM-1 antibody (CD31, R&D systems, cat. no. AF3628, RRID:AB_2161028)
- Alexa Fluor 594 AffiniPure fab fragment goat anti-mouse IgG1, Fcγ fragment specific (Jackson Immuno Research, cat. no. 115-587-185, RRID:AB_2632539)
- Alexa Fluor 594 AffiniPure fab fragment goat anti-mouse IgG2a, Fcγ fragment specific (Jackson Immuno Research, cat. no. 115-587-186, RRID:AB_2632540)
- Alexa Fluor 647 AffiniPure fab fragment goat anti-mouse IgG1, Fcγ fragment specific (Jackson Immuno Research, cat. no. 115-607-185, RRID:AB_2632544)
- Alexa Fluor 647 AffiniPure fab fragment goat anti-rabbit IgG, Fc fragment specific (Jackson Immuno Research, cat. no. 111-607-008, RRID:AB_2632470)

Imaging reagents

- Agarose for agarose–CUBIC-R+(N) gel (Nacalai Tesque, cat. no. 01163-76)
  ▲ **CRITICAL** The gelation characteristics of agarose exhibit variations depending on the manufacturer. To ensure accurate replication of the findings, it is crucial to employ the specific agarose recommended by the designated vendor. Incompatibility between CUBIC and agarose choices may result in unsuccessful gel formation or transparency. In instances where the recommended agarose is unavailable, suitable alternatives include high melting point agarose or high-strength agarose.
- Mineral oil (Sigma-Aldrich, cat. no. M8410)
- HIVAC-F4 (Shin-Etsu Chemical, cat. no. HIVAC-F4) (If not available, silicone oil with a higher RI than the desired RI can be used)

Equipment

Tissue clearing

- 50 ml conical tube (Corning, cat. no. 352070 or Greiner, cat. no. 227261)
- Nunc cell culture treated multidishes (six wells; Thermo Scientific, cat. no. 140675)
  ▲ **CRITICAL** The size of the wells varies depending on the model number of the multiwell plate. In such cases, the device might not fit. We have confirmed that the insert tissue clearing device fits Corning PureCoat Amine 6-well plates, cat. no. 356721. However, other plates may have slight variations in size and require fine-tuning of the design.
- Tight box no. 4 shallow type 1.5 L (as-1, cat. no. 250324)
- Sterile V-bottom free-standing tube 15 ml (Sarstedt, cat. no. 63-2977-90) for immunostaining step
- Protein LoBind tubes 0.5 ml (Eppendorf, cat. no. 0030 108.094)
- 23G intravenous injection needle, butterfly type (Terumo, cat. no. SV-23CLK)
- 26G×1/2″ injection needle (Terumo, cat. no. NN-2613S)
- T shape stopcock (Terumo, cat. no. TS-TL2K)
- 10 ml or 20 ml disposable syringe (Terumo, cat. no. SS-1010SZ, SS-20ESZ)
- Incubation devices. We use hybridization incubator (Taitec, model no. HB-80) or incubator (Eyela, model no. FMS-1000 or MHS-2000)
- Shaker (Taitec, model no. Wave-PR or MixerXR-36)
- Magnetic stirrer
- Hot stirrer
- Water bath

- Abbe refractometer (ATAGO, DR-A1)
- pH meter (Horiba scientific, model no. LAQUA twin)
- Microwave oven
- Fume hood
- Bottle top dispenser (DLAB, cat. no. 2-3828-02)
- Aspirator (Nichimate, ASPIRATORIIa, cat. no. 00-NASP-2A)

3D printer-related equipment to create the tissue clearing devices

- Phrozen Shuffle 2019 XL (Phrozen)
- Formlabs Form Wash (Formlabs)
- Formlabs Form Cure (Formlabs)
- Siraya Tech Blu (Siaya Tech)

Customized light-sheet fluorescence microscope and operation computer

- Optical table with tapped holes (HERZ, model no. h-TDIS-169LA(Y) M6-25XY tap, optimized)
- Compressor (SIGMAKOKI, model no. PC-10H-S)
- Laser (Cobolt, cat. nos. 0488-06-01-0200-100, 488 nm, 200 mW, Cobolt, 0532-04-51-0700, 532 nm, 300 mW, MPB, VFL-P-592-300-OEM1-B1, 592 nm, 300 mW, MPB, VFL-P-647-300-OEM1-B1, 647 nm, 300 mW)
- Optical post (Thorlabs, cat. nos. TR50/M (16×), TR20/M (2×), TR30/M (2×), RS3.5P_M (4×), RS75P4 (4×), RS1P4 (4×), RS 2P4 (4×), RS4P4 (4×), RS-KIT/M (1×))
- Vertical bracket (Thorlabs, cat. no. VB01B/M)
- Lens tube (Thorlabs, cat. no. SM1L40 (2×))
- Post holder (Thorlabs, cat. no. PH50/M (16×))
- ER assembly rods (Thorlabs, cat. nos. ER2 (12×), ER4 (12×) and ER12 (8×))
- Lens mount (Thorlabs, cat. no. CXY1A (4×))
- Cage adapter (Thorlabs, cat. no. LCP33/M (4×))
- Mirror mount (Thorlabs, cat. nos. KCB1C/M (4×), KCB2EC/M (1×), FMP1/M (1×))
- Cage cube (Thorlabs, cat. no. C6WR (1×))
- Base adaptor (Thorlabs, cat. no. BE1/M (10×))
- Camp fork (Thorlabs, cat. no. CF125C/M (10×))
- 1″ Lens tube (Thorlabs, cat. nos. SM1V15 (4×), SM1L30 (4×))
- 1″ Lens tube clamp (Thorlabs, cat. no. SM1RC/M (8×))
- 2″ Lens tube (Thorlabs, cat. nos. SM2L03, SM2L05, SM2CPL05, SM2CPL10)
- Screw conversion adapter (Thorlabs, cat. no. SM2A54)
- Clear-edge flexure mount for Ø1″ (Thorlabs, cat. no. PFM1/M (4×))
- Best form lens (Thorlabs, cat. nos. LBF254-040-A (4×), LBF254-100-A(4×))
- Dielectric mirror (Thorlabs, cat. no. BB1-E02-10 (10×))
- Dichroic mirror (Edmund Optics, cat. nos. 84-746, 84-747, 84-753)
- Glass window (Thorlabs, cat. no. WG12012-A)
- Tunable lens (Edmund Optics, cat. no. 88-937)
- Achromatic doublet lens (Thorlabs, cat. nos. AC254-050-A (2×), AC254-200-A (2×))
- Iris (Thorlabs, cat. no. CP20S (2×))
- Galvano mirror (CItizen, cat. no. 6240H (2×), Thorlabs, cat. no. GCM001 (2×))
- Imaging lens (Edmund Optics, cat. nos. 36-401, 11-149)
- Filter wheel (Edmund Optics, cat. nos. 59-769,59-783,59-772)
- 2″ Emission filter (Edmund Optics, cat. nos. 84-746,84-747,84-753)
- Stepper motor (Orientalmotor, cat. nos. AZM15AK,AZD-AD,CC030VZF)
- Pitch and yaw accessory tilt platform (Thorlabs, cat. no. PY003/M)
- Right angle post clamp (Thorlabs, cat. no. RA90/M)
- Illumination lens (Olympus, cat. no. MVXPLAPO 1X (2×))
- Objective lens (Olympus, cat. no. MVXPLAPO 063X (1x×))
- *XY*-stage (KOHZU, cat. no. YA16A-R101)
- *Z*-stage (KOHZU, cat. no. XA16A-R101)
- Focus-stage (Orientalmotor, cat. no. EAS6RX-D020-AZMKD)

- Sample holder (custom ordered, made of aluminum, anodized black. stl files are available from Supplementary Data 1)
- Left–right switch adapter (created by 3D printer)
- Jigs: Z bracket (MVX10), stage (MVX10), FW-adapter (MVX10), made of black anodized aluminum (MISUMI). Two-dimensional (2D) drawings or stl files are available from Supplementary Data 1)
- Antivibration table (Herz, cat. no. TDIS-169LA(Y), 1,600 × 900)
- Compressor for antivibration table (Sigma, cat. no. PC-10H-S)
- Encoder (Renishow, cat. nos. V2BCY10D10F, A-6195-0100, A-9715-0010; resolution, 0.1 µm)
- Motion driver board (Contek, cat. nos. SMC-8DL-PE, PCB100PS, CCB-SMC2)
- Analog output board (Contek, cat. nos. AO-1616L-LPE, PCB50PS-1.5P, EPD-50A)
- NPN (negative–positive–negative) transistors (NEC, cat. no. C4552. Alternatives are possible)
- Potentiometer (TOCOS, cat. no. GF063P, 1 kΩ. Alternatives are possible)
- Power supply (GW Instek, cat. no. GPE-3323 (2×))
- Customized sample chamber (LINKS, inner size: W 110 mm × D 100 mm × H 175 mm, aluminum black anodized aluminum)
- Customized sample holder (LINKS, inner size: W 50 mm × H 70 mm × 1 mm)
- Zoom body (Olympus, model no. MVX10)
- sCMOS (scientific complementary metal–oxide–semiconductor) camera (Hamamatsu Photonics, Orca-Fusion)
- Microscope control PC (Japan computing systems, Windows 10 Pro 64 bit, CPU: Intel Core i9 10980XE, memory: DDR4-2400 16 GB (4×), M.2. SSD (240 GB, 4 TB))
- Visual Studio Community 2022 for creating microscope control software (C++/CLI)

Data analysis tools

- Computer ((Customized, Windows 11 Pro 64 bit, CPU: Intel Core i9 13900 KS, memory: DDR5-4600 32 GB (4×), M.2. SSD (930 GB), storage 550 TB), GPU: GeForce RTX3090)
- ImageJ (free software from the US National Institutes of Health)
- Python 3.11
- CUDA Toolkit 12.3
- CUBIC-Cloud (https://cubic-cloud.com/)
- CUBIC-Atlas version 1.2 (http://cubic-atlas.riken.jp)

Reagent setup

PBS: dissolve a PBS tablet with 1 L of dH_2O.
PBS/NaN_3 (0.01% wt/vol): for example, to prepare 1 L, dissolve 0.1 mg sodium azide with 1 L of PBS.

CUBIC-L: CUBIC-L solution consists of a mixture of 10% (wt/wt) *N*-butyldiethanolamine and 10% (wt/wt) Triton X-100 dissolved in dH_2O. To prepare 1000 g of CUBIC-L solution, 100 g of *N*-butyldiethanolamine and 100 g of Triton X-100 in 800 g of dH_2O are mixed thoroughly using a magnetic stirrer at room temperature (approximately 25 °C). The solution can be stored at room temperature for up to 12 months. Alternatively, CUBIC-L solutions are commercially available.

CUBIC-R+(N): CUBIC-R+(N) consists of a mixture of 45% (wt/wt) antipyrine, 30% (wt/wt) nicotinamide, 0.5% (vol/vol) *N*-butyldiethanolamine and dH_2O. To prepare 1,000 g of CUBIC-R+ solution, 450 g of antipyrine and 300 g of nicotinamide are dissolved in 250 g of dH_2O. After complete dissolution, 2.5 ml of *N*-butyldiethanolamine is added to the 1,000 ml solution to give a pH of 9.6–9.8 and a RI of 1.522. The CUBIC-R+(N) solution can be stored at room temperature for up to 6 months.

3% H_2O_2 solution: hydrogen peroxide solution is diluted 10 times with dH_2O. For example, to prepare 100 ml of 3% H_2O_2, 10 ml of H_2O_2 was mixed with 90 ml of dH_2O.

1% formalin (FA) solution for post-fixation of immunostaining: 37% formaldehyde solution was 37 times diluted with PBS. For example, to prepare 100 ml of 1% FA solution, 2.7 ml of FA was mixed with 97.3 ml of PBS.

Equipment setup

Construction of the customized light-sheet microscopy system

Construct a simple and rapid customized digital scan light-sheet microscopy system for 3D fluorescence imaging of entire cleared organs (Supplementary Fig. 5 and Supplementary Data 1)[53]. To rapidly observe sparse and target signals across the entire mouse organ, a 0.63× objective lens is used to provide a wide field of view. Different lenses can be used as needed. When using a high NA objective lens, it is necessary to be aware of the loss of resolution due to aberrations caused by differences in RI between oil, sample and air, and defocusing due to narrow focal depth. The sensor uses Orca-Fusion, known for its high quantum efficiency and rapid imaging capability (89.1 frames/s at 2,304 × 2,304 resolution, quantum efficiency: 80%). Four-color lasers are individually collimated using best form lenses (f40 and f100). The distance between the lenses is ideally 140 mm but is adjusted according to the divergence of each beam. These collimated lasers are then combined into a single optical path via dichroic mirrors. Switching of the left and right paths is done using mirrors attached to a stepper motor. On each side, the lasers are expanded using achromatic lenses with focal lengths of $f = 50$ and $f = 200$. The distance between these two lenses adjusts to 250 mm. Using the cage system, the lens are mounted in a kinematic lens holder to prepare for adjustment. To correct and adjust the light sheet focus, for chromatic aberrations and RI discrepancies in the light sheet caused by lenses and oil, a plano-concave lens($f = -100$) and a tunable lens are placed in front of the galvanometer mirror. The galvanometer mirror is placed at the back focal point of the illumination objective lens. In the sample chamber, a cylindrical lens made of BK-7, which is close to the RI of immersion oil (RI of 1.522), is used to reduce aberrations[67]. The current for tunable lens control is controlled using an analog input/output device and NPN transistors, which are used for remote focusing of the light sheet by computer. Irises were placed before the tunable lens to adjust the *z*-resolution. To simplify sample handling, an observation system is set up below the chamber. As the zoom body is placed under the antivibration table, it is connected to a stepper motor so that the magnification can be changed by software control. For *z*-stack imaging, we used the MOVIE-scan method[47]. The control software for imaging and reconstruction is developed in C++/CLI using Visual Studio. Synchronization between devices is important for the MOVIE system, and low-level language coding is preferred.

Preparation of tissue clearing insert devices

The tissue clearing insert devices were formed with a 3D printer using the CAD files in Supplementary Data 2. After forming, excess resin was washed with isopropanol (form wash) and secondary curing was performed (form cure). The supports were removed by nipper.
▲ **CAUTION** If the supports are not completely removed, the broken end of the support may damage the sample.

Procedure

MK-801 and haloperidol administration

● **TIMING 9 h**

1. Dissolve MK-801 in saline to a concentration of 250 µg/ml, and dissolve 5 mg of haloperidol in 50 µl of 3 M acetic acid solution and adjust it to 125 µg/ml with saline.
   (A) **Administer the solutions via intraperitoneal injection**
      (i) Use a volume of 200 µl per mouse, resulting in doses of 2 mg/kg for MK-801 and 1 mg/kg for haloperidol, assuming a mouse weight of 25 g.
      (ii) Initially, inject 200 µl of either MK-801 or saline intraperitoneally using a 26 gauge, 1/2 inch needle.
      (iii) After 3 h, inject 200 µl of either haloperidol or saline using a 26 gauge, ½ inch needle.
      (iv) Perform perfusion fixation 3 h after the final administration.

Dissection

● **TIMING 10–15 min**

2. Induce deep anesthesia in the mouse.
   (A) **Use pentobarbital (~150 mg/kg of body weight) or a combination of ketamine (100 mg/kg of body weight) and xylazine (10 mg/kg of body weight)**
      (i) Perform an intraperitoneal (i.p.) injection, using 1 ml syringe with a 26 gauge, ½ inch injection needle or by employing isoflurane.
      (ii) Following anesthesia, perfuse the mouse with 20 ml of cold to eliminate blood of the organs.
      (iii) Subsequently, perfuse with 20 ml of cold 4% PFA at a rate below 10 ml/min.
      (iv) To avoid damaging the sample, care should be taken when dissecting the entire brain or other organs using scissors or tweezers.

Fixation

● **TIMING 0.5–1 d**

3. Post-fix the dissected organs by immersing them in 7.5 ml of 4% PFA and gently shaking at 4 °C for 12–24 h.
   ▲ **CRITICAL STEP** It is crucial to strictly adhere to the specified fixation duration and temperature to prevent overfixation. Prolonged fixation (e.g., >2 d or at elevated temperatures) may result in decreased transparency and some antigenicity decrease.

PBS wash

● **TIMING 0.5 d**

4. Wash the fixed organs three times with 7.5 ml of PBS/NaN_3 (0.01% wt/vol) for a minimum of 2 h at room temperature to eliminate any remaining PFA.

Tissue clearing

● **TIMING 13–16 d**

5. Follow the process for either 1/2 diluted or undiluted CUBIC-L treatment.
   (A) **1/2-diluted CUBIC-L treatment**
      (i) Immerse the fixed organ in 7.5 ml of 1/2-diluted CUBIC-L with gentle shaking at 37 °C for at least 6 h (Fig. 3b).
      ■ **PAUSE POINT** Overnight incubation is also allowed.
   (B) **CUBIC-L treatment**
      (i) Exchange the 7.5 ml of CUBIC-L solution and continue gently shaking at 37 °C for 6 d.
      (ii) Refresh the CUBIC-L every 2 d.
      ▲ **CRITICAL STEP** The CUBIC-L treatment is complete when the organ appears translucent white.
      ▲ **CAUTION** Be careful when aspirating reagents because organs treated with CUBIC-L become soft, and aspiration should be performed from a designated area and not directly touching the sample.
      ▲ **CRITICAL STEP** For smaller organs, such as the eye, less than 6 d of delipidation is sufficient to obtain sufficient transparency. The delipidation period can be adjusted depending on the organ.
   (C) **PBS wash**
      (i) Stop the delipidation reaction and remove the residual CUBIC-L reagent by washing with 7.5 ml of PBS for a minimum of 2 h at room temperature with gentle agitation.
      (ii) Repeat this washing procedure at least three times.
      ◆ **TROUBLESHOOTING**
      ■ **PAUSE POINT** Organs treated with CUBIC-L can be stored in PBS/0.01% wt/vol sodium azide at 4 °C for a maximum of 1 week. Following storage, resuming staining or RI matching steps can be done without the need for additional procedures.
   (D) **Melanin decolorization (optional)**
      For organs with abundant pigments, such as the eye, decolorize using hydrogen peroxide after delipidation.

(i) Dilute hydrogen peroxide (~30%) to 3% with dH_2O and gently agitate at 37 °C for at least a day. If decolorization is insufficient, exchange the hydrogen peroxide daily, repeating for several days.

(ii) Wash the samples in 7.5 ml of PBS at 37 °C for at least 2 h, repeating the washing process three times (overnight washes are also allowed).

(E) **Nuclear staining (optional)**

(i) Wash the delipidated organs with 7.5 ml of CUBIC-HV nuclear staining buffer.

(ii) Exchange the buffer with CUBIC-HV nuclear staining buffer containing a nuclear staining reagent (PI: 120 µl, RD2: 30 µl of 200× solution, SYTOX-G: 1.8 µl dissolved in 7.5 ml of staining buffer) and gently shake at 37 °C for 3 d. You can optimize the staining duration based on the tissue size. After staining, wash the samples with 7.5 ml of PBS at 37 °C for at least 2 h, repeating at least three times (overnight washes are also allowed).

(F) **Immunostaining (optional)**

(i) For immunostaining of the brain, this step involves transferring the sample to a 15 ml free-stand tube.

(ii) Replace the sample in the staining reagent of CUBIC-HV immunostaining buffer at 25 °C for 1.5 h. During this time, preincubate the primary and secondary antibodies. After binding the secondary antibody (2/3 the amount of primary antibody) with primary antibodies (NeuN: 7.5 µg/brain, c-Fos: 1.0 µg/brain, PV: 1.0 µg/brain, α-SMA: 2.0 µg/brain, 0.4 µg/eye, CD31: 10.0 µg/brain, 2.0 µg/eye), gently shake the sample in 500 µl of staining solution at 25 °C for 1–4 weeks. For example, incubate NeuN, α-SMA and CD31 for 1 week, and costain PV and c-Fos for 4 weeks. Adjust the reaction temperatures and durations according to the sample and antibody.

(iii) Incubate at 4 °C for 1 d.

(iv) Wash the sample with 3D immunostaining wash buffer for at least 2 h, repeating at least three times.

(v) Perform post-fixation with 1% FA solution at 4 °C for 1 d.

(vi) Wash the samples in PBS 7.5 ml at 37 °C for at least 2 h, repeated for a minimum of three times (overnight washes are also allowed).

▲ **CAUTION** In the case of mouse brain, perform immunostaining in a suitable tube with a rounded bottom (Sarstedt, cat. no. 63-2977-90) and fix the tube vertically in the same shaker used for the tube-based CUBIC-L treatment (Fig. 3e). Set the shaker to 45 rpm, as vigorous agitation may damage the sample.

(G) **1/2-diluted CUBIC-R+(N) treatment**

(i) Immerse the sample in 7.5 ml of 1/2-diluted CUBIC-R+(N) with gentle shaking at room temperature for at least 6 h (overnight immersion is also allowed).

(H) **CUBIC-R+(N) treatment**

(i) Immerse the sample in 7.5 ml of CUBIC-R+(N) and gently shake it at room temperature overnight. The following day, replace the reagent with fresh and continue incubation for an additional 24 h.

■ **PAUSE POINT** Cleared organs can be stored in CUBIC-R+(N) at room temperature. The duration of maximum storage is depending on the staining dye. To prevent sample crystallization, refrain from storing at 4 °C. For extended storage, immerse the samples in CUBIC-R+(N) following gel embedding and store in dark.

▲ **CAUTION** When using with fluorescent protein-labeled organs, prolonged storage in CUBIC-R+(N) may decrease the signal intensity, thus, it is advisable to avoid storage.

Gel embedding

● **TIMING 1 d**

6. Follow the process for the preparation of CUBIC–agarose and sample embedding.

(A) **Agarose–CUBIC-R+(N) reagent preparation**

(i) Before heating, add 2 wt% agarose powder to CUBIC-R+(N) at room temperature and ensure thorough diffusion with vigorous shaking. For example, to prepare

six samples for embedding, add 2 g of agarose to 98 g of CUBIC-R+(N) solution in a capped glass bottle. Heat the well-diffused agarose–CUBIC-R+(N) mixture in a microwave until it reaches boiling point. Ensure to loosen the bottle cap before heating. Once removed from the microwave, shake the bottle vigorously after recapping. Repeat the microwave heating and shaking process several times until the agarose is completely dissolved.

▲ **CRITICAL STEP** Checking whether agarose–CUBIC-R+(N) mixture becomes clear is important when determining whether it is dissolved.

◆ **TROUBLESHOOTING**

▲ **CAUTION** Tightly closed bottles should not be heated in a microwave oven because of the risk of rupture.

(B) **Defoaming of the gel**

(i) Incubate the agarose–CUBIC-R+(N) solution bottle in a hot water bath at 60 °C for at least 30 min to remove bubbles in agarose–CUBIC-R+(N) solution.

(C) **First gel layer preparation**

(i) Filling 10 ml of agarose–CUBIC-R+(N) solution into each well with a 10 ml pipette. Carefully remove any air bubbles with a 1 ml micropipette before viscosity increases. Then cover the agarose–CUBIC solution with a lid and stand at 4 °C for 20 min. If the agarose–CUBIC-R+(N) solution does not gel, incubate further at 4 °C.

▲ **CRITICAL STEP** The orientation of the sample is important for imaging with a light-sheet microscope. Be sure to move the plate carefully during the gel embedding process to ensure that the sample does not move from its intended orientation.

▲ **CRITICAL STEP** To keep the agarose–CUBIC-R+(N) solution at 60 °C, return the agarose–CUBIC solution bottle to the hot water bath immediately after pouring.

▲ **CRITICAL STEP** Since agarose–CUBIC-R+(N) is easily crystallized by evaporation of water, capping is necessary for incubation.

▲ **CRITICAL STEP** Longer incubation such as several hours at 4 °C can make samples crystallize. Time keeping and frequent checking are essential.

▲ **CRITICAL** If air bubbles remain in the gel, they can cause artifacts during imaging. It is important to remove air bubbles completely.

▲ **CRITICAL** If a lower temperature gel is desired, low-melting-point agarose may be used, but it should be noted that it is difficult to gel.

◆ **TROUBLESHOOTING**

(D) **Second gel layer preparation**

(i) Fill the wells with agarose–CUBIC-R+(N) solution and completely embed the sample. Carefully remove any air bubbles and incubate at room temperature for at least 6 h.

Setting a sample for microscopy

● **TIMING 1–2 h**

7. Contamination of CUBIC+R(N) in the oil in the chamber can cause artifacts during imaging. To avoid contamination:

(i) When transferring the gel into the chamber, replace it with oil to avoid contaminating the CUBIC-R+(N) reagent.

(ii) When performing volumetric imaging, it is essential to set the sample as symmetrically as possible.

(iii) It is also important to consider the thickness of the organ and the direction of imaging.

◆ **TROUBLESHOOTING**

Imaging

● **TIMING 0.5–1 h per sample**

8. Set the magnification to the appropriate magnification for the sample to determine the imaging range (left, right, up, down and depth directions).

(A) **Set the laser output and exposure time to obtain conditions that provide sufficient signal-to-noise ratio for data analysis**

(i) For multicolor imaging, set the laser wavelength, power, optical filter and exposure time respectively.

(ii) Setting the *xy* resolution equal to the *z* step on imaging will simplify positioning for subsequent analysis.

◆ **TROUBLESHOOTING**

▲ **CRITICAL STEP** Adjustment must be quickly done because too much time taken to set the positioning and acquisition conditions will cause some of the samples to fade.

Data analysis

● **TIMING 1 d**

9. For implementation ease, the program is written in Python and utilizes the Cupy, Numba and OpenCV libraries to increase computation performance.

(A) **Software setup**

(i) First, download and install Python3 for the user's OS (https://www.python.org/downloads/). In addition, run the following command in the working directory to install the required Python:

(ii)
```
pip install -r requirements.txt
```

If the appropriate software such as Python3, Pip including CUDA-toolkit are installed, the required packages will be installed successfully. Conflicts may occur and it may not install or work properly adjustments must be required.

(B) **Cell detection**

(i) Place the attached PointDetection.py and CellDetection.ipynb in the same folder and run CellDetection.ipynb. The folder containing the image files for each channel (Structure, color1, color2) is placed under the parent folder path in 'FP'.

(ii) 'params' is an array of four numbers: the background value, the minimum signal-to-noise ratio to be detected as a peak, the maximum point shape-like value (the smaller, the more rigorous) and the minimum difference between the peak and the minimum value in the neighborhood (deltaI).

(iii) 'zsize' is the number of images to be computed by the GPU at one time, which is determined by the GPU memory size and the size of the image. The 'overlap' should be set to at least twice the 'peak_size'. This is because the edges of the image are not calculated accurately.

(iv) 'peak_size' is the kernel size of the maximum filter and is adjusted to about the size of one cell. Smaller values allow for more closely spaced signals to be resolved.

(v) 'psf_sigmas' is a parameter that creates the desired cell shape and can be set to multiple patterns. The order is (*z*,*y*,*x*), setting a larger value for *z* if the *z* resolution is poor. 27 different subpixel point images are obtained with one parameter and compared to the normalized value of each peak.

(vi) The detected cells are output as a CSV file and point image (Gaussian filtered) as TIFF format.

(vii) The point images can be compared with the raw images using software such as ImageJ to confirm that the cells were detected correctly.

◆ **TROUBLESHOOTING**

▲ **CRITICAL STEP** If the folder hierarchy is not correctly arranged, an error will arise.

(C) **Data analysis using CUBIC-Cloud**

(i) Log in to CUBIC-Cloud and select '+NEW' under 'Database' and upload 'coordinates_um.csv' and 'Structure_image.tif' to CUBIC-Cloud. Each file name is arbitrary.

(ii) After uploading, the status becomes 'process' and starts mapping to CUBIC-Atlas. When the process is completed successfully, 'OK' is displayed. After all samples are successfully uploaded, analysis of the data can be performed.

(iii) The cell coordinates, number of cells in each region and other data after mapping to CUBIC-Atlas can be downloaded from the 'Download'. This enables more detailed analysis and drawing at the local computer.
(iv) To analyze and visualize the data, create a notebook for the analysis by clicking '+NEW' in the 'My list' of the Notebooks.
(v) '+Add group' to create a sample group name and select samples.
(vi) After setting up the group, click '+Add graph' to enter the graph type, sample group and parameters, and the image will be displayed.
(vii) The images and graphs can be downloaded as PNG, SVG or CSV format.
(viii) In 'Studios', you can view a 3D image of each sample or group of samples and download movies.
◆ **TROUBLESHOOTING**

Troubleshooting

Troubleshooting advice can be found in Table 1.

Table 1 | Troubleshooting table

Step	Problem	Possible reason	Possible solution
Reagent setup	Casein is not dissolved in CUBIC-HV staining buffer	Insufficient stirring time or strength	Heat in the microwave oven until just before boiling, then stir gently with a stirrer
	Crystallization of CUBIC-R+(N) reagent	Decrease in solubility due to evaporation of water or decrease in temperature	Check and adjust the RI value and adjust with dH_2O to 1.522 and heat to room temperature
Preparation of tissue clearing insert devices	Failure of forming	Not enough support or bad forming conditions	Add support settings in the slicer software and check the forming conditions such as speed and exposure time
	Device and wells do not match in size	Well size varies from each vendor	Use recommended multiwell plates or change the design of the device
5 (tissue clearing)	Liquid volume decreases during incubation	Insufficient sealing	Seal the multiwell plate in tupperware
	Insufficient delipidation of organs	Not enough shaking	Change the shaker setting to mix the reagents in the wells
		Insufficient period of delipidation	Extend the period of delipidation
5 (decolorization)	Bubbles are generated in the sample during decolorization	Incubation temperature is high, or hydrogen peroxide concentration is high	Reduce the temperature of incubation to room temperature or reduce the concentration of hydrogen peroxide to 1%
5 (RI matching)	Not enough transparency	Insufficient delipidation with CUBIC-L	Extend the duration of delipidation
		RI matching is not complete	Replace with new CUBIC-R+(N) and further incubate
		RI of the CUBIC-R+(N) is decreasing	Replace with new CUBIC-R+(N)
6 (gel embedding)	Organs are displaced from the center	The platform on which the plates are placed is not level	Place on a level table
	Organs are sticking out of the gel	Insufficient amount of gel solution of the first layer	Fill the gel solution until the organ is completely covered. If the solution is reduced when the air bubbles are drained, add more gel solution
	Gel chipping when pulling out the device	Pulling the device straight up	While rotating the device, pull it out so that there is a gap between it and the well
7 (setting a gel sample for microscopy)	Gel moves on imaging table	Imaging table is not level	Level the imaging table
	Immersion oil for photography is cloudy	CUBIC-R+(N) is mixed in the oil	Place the oil through once in a separately prepared oil before transferring to the immersion oil

Table 1 (continued) | Troubleshooting table

Step	Problem	Possible reason	Possible solution
8 (imaging)	Low intensity in the center	Staining is too intense	Dilute the dye or slightly shift the excitation wavelength away from the absorption peak
	Poor *z*-resolution	If the entire image has low resolution, it may be due to the input laser being too thin	Increase the diameter of the input laser
		If only a part of the image has high resolution, it indicates that the input laser is too thick	Reduce the diameter of the input laser
9 (data analysis)	Low detection accuracy	Wrong psf parameters	Change or add the sigma values
	Failure to upload to the CUBIC-Cloud	Wrong cell coordinate file	Check that it does not contain column numbers and that it is in μm units
		Wrong resolution of structural image	Create an image with the appropriate resolution
	Failure to create a spatial heat map or *P* value map	Too small grid values or diameter	Change parameters
	Overlapping text on the graph	Too many regions are selected	Reduce the number of regions or adjust the row and column numbers
			Export as SVG format and adjust with appropriate software such as Adobe Illustrator
	Unable to download images	The image has timed out	Reload the browser

Timing

Step 1 MK-801 + haloperidol administration: 9 h
Step 2 Dissection: 10–15 min
Step 3 Fixation: 0.5–1 d
Step 4 PBS wash: 0.5 d
Step 5 (A–C) Delipidation: 7–8 d
Step 5 (D) Melanin decolorization: 1–2 d (optional)
Step 5 (E) Nuclear staining: 3 d
Step 5 (F) Immunostaining: 14–28 d
Step 5 (G,H) RI matching: 3 d
Step 6 Gel embedding: 1 d
Step 7 Setting a sample for microscopy: 1–2 h
Step 8 Imaging: 0.5–1 h per sample
Step 9 Data analysis: 1 d

Anticipated results

This high-throughput tissue clearing protocol, which combines a multiwell plate with a tissue clearing insert device, enables parallelization of the tissue clearing process by streamlining the complex task of reagent exchange. Even with this protocol, the transparency was comparable to the conventional method using conical tubes and it enables the parallel clearing of not only the brain but also most organs in mice (salivary gland, heart, lung, spleen, kidney, testis) (Fig. 4c,d and Supplementary Fig. 1). Additionally, even in organs with abundant pigments, such as the eye, clearing is achieved by addition to decolorization step using hydrogen peroxide. Furthermore, even decolorization with hydrogen peroxide allow immunostaining.

Here, as an example, we showed that changes in neuronal activity induced by drug administration can be analyzed over the entire region of the mouse brain by using CUBIC-Cloud

to analyze changes in neuronal activity stained by anti-c-Fos antibodies for whole brains. This high-throughput tissue clearing protocol will make it easier than ever to compare and observe phenomena of interest throughout the entire brain, such as changes in neural activity due to drug administration or various stimulations.

Data availability

CUBIC-Atlas reference data are available from http://cubic-atlas.riken.jp. Other datasets generated or analyzed during the current study are available from the corresponding author on reasonable request. Source data are provided with this paper.

Code availability

All source codes for cell detection are available in the Supplementary Data. Source codes of microscope and MOVIE system are available from the corresponding author on reasonable request.

Received: 7 January 2024; Accepted: 25 September 2024;
Published online: 03 December 2024

References

1. Lundvall, H. Weiteres über demonstration embryonaler Skelette. *Anat. Anz.* **27**, 520–523 (1905).
2. Spalteholz, W. *Über das Durchsichtigmachen von Menschlichen und Tierischen Präparaten* (S. Hirzel, 1914).
3. Bakutkin, V. V., Maksimova, I. L., Semyonova, T. N., Tuchin, V. V. & Kon, I. L. Controlling of optical properties of sclera. *Proc. SPIE* **2393**, 137–141 (1995).
4. Tuchin, V. V. et al. Light propagation in tissues with controlled optical properties. *J. Biomed. Opt.* **2**, 401–417 (1997).
5. Dodt, H. U. et al. Ultramicroscopy: three-dimensional visualization of neuronal networks in the whole mouse brain. *Nat. Methods* **4**, 331–336 (2007).
6. Erturk, A. et al. Three-dimensional imaging of the unsectioned adult spinal cord to assess axon regeneration and glial responses after injury. *Nat. Med.* **18**, 166–171 (2011).
7. Chung, K. et al. Structural and molecular interrogation of intact biological systems. *Nature* **497**, 332–337 (2013).
8. Hama, H. et al. ScaleS: an optical clearing palette for biological imaging. *Nat. Neurosci.* **18**, 1518–1529 (2015).
9. Hama, H. et al. Scale: a chemical approach for fluorescence imaging and reconstruction of transparent mouse brain. *Nat. Neurosci.* **14**, 1481–1488 (2011).
10. Tainaka, K. et al. Whole-body imaging with single-cell resolution by tissue decolorization. *Cell* **159**, 911–924 (2014).
11. Susaki, E. A. et al. Whole-brain imaging with single-cell resolution using chemical cocktails and computational analysis. *Cell* **157**, 726–739 (2014).
12. Ueda, H. R. et al. Tissue clearing and its applications in neuroscience. *Nat. Rev. Neurosci.* **21**, 61–79 (2020).
13. Ueda, H. R. et al. Whole-brain profiling of cells and circuits in mammals by tissue clearing and light-sheet microscopy. *Neuron* **106**, 369–387 (2020).
14. Richardson, D. S. et al. Tissue clearing. *Nat. Rev. Methods Prim.* **1**, 84 (2021).
15. Nojima, S. et al. CUBIC pathology: three-dimensional imaging for pathological diagnosis. *Sci. Rep.* **7**, 9269 (2017).
16. Yang, B. et al. Single-cell phenotyping within transparent intact tissue through whole-body clearing. *Cell* **158**, 945–958 (2014).
17. Erturk, A. et al. Three-dimensional imaging of solvent-cleared organs using 3DISCO. *Nat. Protoc.* **7**, 1983–1995 (2012).
18. Renier, N. et al. iDISCO: a simple, rapid method to immunolabel large tissue samples for volume imaging. *Cell* **159**, 896–910 (2014).
19. Kurihara, D., Mizuta, Y., Sato, Y. & Higashiyama, T. ClearSee: a rapid optical clearing reagent for whole-plant fluorescence imaging. *Development* **142**, 4168–4179 (2015).
20. Tomer, R., Ye, L., Hsueh, B. & Deisseroth, K. Advanced CLARITY for rapid and high-resolution imaging of intact tissues. *Nat. Protoc.* **9**, 1682–1697 (2014).
21. Pan, C. et al. Shrinkage-mediated imaging of entire organs and organisms using uDISCO. *Nat. Methods* **13**, 859–867 (2016).
22. Erturk, A. & Bradke, F. High-resolution imaging of entire organs by 3-dimensional imaging of solvent cleared organs (3DISCO). *Exp. Neurol.* **242**, 57–64 (2013).
23. Erturk, A., Lafkas, D. & Chalouni, C. Imaging cleared intact biological systems at a cellular level by 3DISCO. *J. Vis. Exp.* https://doi.org/10.3791/51382 (2014).
24. Cai, R. et al. Panoptic imaging of transparent mice reveals whole-body neuronal projections and skull–meninges connections. *Nat. Neurosci.* **22**, 317–327 (2019).
25. Zhao, S. et al. Cellular and molecular probing of intact human organs. *Cell* **180**, 796–812. e719 (2020).
26. Murray, E. et al. Simple, scalable proteomic imaging for high-dimensional profiling of intact systems. *Cell* **163**, 1500–1514 (2015).
27. Kim, S.-Y. et al. Stochastic electrotransport selectively enhances the transport of highly electromobile molecules. *Proc. Natl Acad. Sci. USA* **112**, E6274–E6283 (2015).
28. Miyawaki, A. Fluorescence imaging in the last two decades. *Microscopy* **62**, 63–68 (2013).
29. Tomer, R. et al. SPED light sheet microscopy: fast mapping of biological system structure and function. *Cell* **163**, 1796–1806 (2015).
30. Menegas, W. et al. Dopamine neurons projecting to the posterior striatum form an anatomically distinct subclass. *eLife* **4**, e10032 (2015).
31. Treweek, J. B. et al. Whole-body tissue stabilization and selective extractions via tissue-hydrogel hybrids for high-resolution intact circuit mapping and phenotyping. *Nat. Protoc.* **10**, 1860–1896 (2015).
32. Lane, N. The unseen world: reflections on Leeuwenhoek (1677) 'Concerning little animals'. *Philos. Trans. R. Soc. B* **370**, 20140344 (2015).
33. Vigouroux, R. J., Belle, M. & Chedotal, A. Neuroscience in the third dimension: shedding new light on the brain with tissue clearing. *Mol. Brain* **10**, 33 (2017).
34. Greenbaum, A. et al. Bone CLARITY: clearing, imaging, and computational analysis of osteoprogenitors within intact bone marrow. *Sci. Transl. Med.* **9**, eaah6518 (2017).
35. Ren, Z. et al. CUBIC-plus: an optimized method for rapid tissue clearing and decolorization. *Biochem. Biophys. Res. Commun.* **568**, 116–123 (2021).
36. Park, Y.-G. et al. Protection of tissue physicochemical properties using polyfunctional crosslinkers. *Nat. Biotechnol.* **37**, 73–83 (2018).
37. Hahn, C. et al. High-resolution imaging of fluorescent whole mouse brains using stabilised organic media (sDISCO). *J. Biophoton.* **12**, e201800368 (2019).
38. Qi, Y. et al. FDISCO: advanced solvent-based clearing method for imaging whole organs. *Sci. Adv.* **5**, eaau8355 (2019).
39. Pende, M. et al. High-resolution ultramicroscopy of the developing and adult nervous system in optically cleared *Drosophila melanogaster*. *Nat. Commun.* **9**, 4731 (2018).
40. Messal, H. A. et al. Antigen retrieval and clearing for whole-organ immunofluorescence by FLASH. *Nat. Protoc.* **16**, 239–262 (2021).
41. Susaki, E. A. et al. Advanced CUBIC protocols for whole-brain and whole-body clearing and imaging. *Nat. Protoc.* **10**, 1709–1727 (2015).
42. Tainaka, K., Kuno, A., Kubota, S. I., Murakami, T. & Ueda, H. R. Chemical principles in tissue clearing and staining protocols for whole-body cell profiling. *Ann. Rev. Cell Dev. Biol.* **32**, 713–741 (2016).
43. Kubota, S. I. et al. Whole-body profiling of cancer metastasis with single-cell resolution. *Cell Rep.* **20**, 236–250 (2017).
44. Murakami, T. C. et al. A three-dimensional single-cell-resolution whole-brain atlas using CUBIC-X expansion microscopy and tissue clearing. *Nat. Neurosci.* **21**, 625–637 (2018).
45. Watanabe, T. et al. Comparison of the 3-D patterns of the parasympathetic nervous system in the lung at late developmental stages between mouse and chicken. *Dev. Biol.* https://doi.org/10.1016/j.ydbio.2018.05.014 (2018).
46. Tainaka, K. et al. Chemical landscape for tissue clearing based on hydrophilic reagents. *Cell Rep.* **24**, 2196–2210.e9 (2018).

47. Matsumoto, K. et al. Advanced CUBIC tissue clearing for whole-organ cell profiling. *Nat. Protoc.* **14**, 3506–3537 (2019).
48. Susaki, E. A. et al. Versatile whole-organ/body staining and imaging based on electrolyte-gel properties of biological tissues. *Nat. Commun.* **11**, 1982 (2020).
49. Kuroda, M. & Kuroda, S. Whole-body clearing of beetles by successive treatment with hydrogen peroxide and CUBIC reagents. *Entomol. Sci.* **23**, 311–315 (2020).
50. Mano, T. et al. CUBIC-Cloud provides an integrative computational framework toward community-driven whole-mouse-brain mapping. *Cell Rep. Methods* **1**, 100038 (2021).
51. Perbellini, F. et al. Free-of-acrylamide SDS-based tissue clearing (FASTClear) for three dimensional visualization of myocardial tissue. *Sci. Rep.* **7**, 5188 (2017).
52. Launay, P. S. et al. Combined 3DISCO clearing method, retrograde tracer and ultramicroscopy to map corneal neurons in a whole adult mouse trigeminal ganglion. *Exp. Eye Res.* **139**, 136–143 (2015).
53. Keller, P. J., Schmidt, A. D., Wittbrodt, J. & Stelzer, E. H. Reconstruction of zebrafish early embryonic development by scanned light sheet microscopy. *Science* **322**, 1065–1069 (2008).
54. Silvestri, L., Bria, A., Sacconi, L., Iannello, G. & Pavone, F. S. Confocal light sheet microscopy: micron-scale neuroanatomy of the entire mouse brain. *Opt. Express* **20**, 20582–20598 (2012).
55. Frasconi, P. et al. Large-scale automated identification of mouse brain cells in confocal light sheet microscopy images. *Bioinformatics* **30**, i587–i593 (2014).
56. Silvestri, L. et al. Quantitative neuroanatomy of all Purkinje cells with light sheet microscopy and high-throughput image analysis. *Front. Neuroanat.* **9**, 68 (2015).
57. Silvestri, L. et al. Universal autofocus for quantitative volumetric microscopy of whole mouse brains. *Nat. Methods* **18**, 953–958 (2021).
58. Ahrens, M. B., Orger, M. B., Robson, D. N., Li, J. M. & Keller, P. J. Whole-brain functional imaging at cellular resolution using light-sheet microscopy. *Nat. Methods* **10**, 413–420 (2013).
59. Keller, P. J. & Ahrens, M. B. Visualizing whole-brain activity and development at the single-cell level using light-sheet microscopy. *Neuron* **85**, 462–483 (2015).
60. Seiriki, K. et al. High-speed and scalable whole-brain imaging in rodents and primates. *Neuron* **94**, 1085–1100.e1086 (2017).
61. Liu, Y. C. & Chiang, A. S. High-resolution confocal imaging and three-dimensional rendering. *Methods* **30**, 86–93 (2003).
62. Helmchen, F. & Denk, W. Deep tissue two-photon microscopy. *Nat. Methods* **2**, 932–940 (2005).
63. Chen, B.-C. et al. Lattice light-sheet microscopy: imaging molecules to embryos at high spatiotemporal resolution. *Science* **346**, 1257998 (2014).
64. Dean, K. M., Roudot, P., Welf, E. S., Danuser, G. & Fiolka, R. Deconvolution-free subcellular imaging with axially swept light sheet microscopy. *Biophys. J.* **108**, 2807–2815 (2015).
65. Dean, K. M. et al. Isotropic imaging across spatial scales with axially swept light-sheet microscopy. *Nat. Protoc.* **17**, 2025–2053 (2022).
66. Glaser, A. K. et al. Light-sheet microscopy for slide-free non-destructive pathology of large clinical specimens. *Nat. Biomed. Eng*. https://doi.org/10.1038/s41551-017-0084 (2017).
67. Glaser, A. K. et al. Multi-immersion open-top light-sheet microscope for high-throughput imaging of cleared tissues. *Nat. Commun.* **10**, 2781 (2019).
68. Glaser, A. K. et al. A hybrid open-top light-sheet microscope for versatile multi-scale imaging of cleared tissues. *Nat. Methods* **19**, 613–619 (2022).
69. Ryan, D. P. et al. Automatic and adaptive heterogeneous refractive index compensation for light-sheet microscopy. *Nat. Commun.* **8**, 612 (2017).
70. Renier, N. et al. Mapping of brain activity by automated volume analysis of immediate early genes. *Cell* **165**, 1789–1802 (2016).
71. Furth, D. et al. An interactive framework for whole-brain maps at cellular resolution. *Nat. Neurosci.* **21**, 139–149 (2018).

Acknowledgements

We thank the people at RIKEN and The University of Tokyo, in particular E. A. Susaki and S. Y. Yoshida for helping with immunostaining and data analysis. This work was supported by a JST ERATO grant (H.R.U., no. JPMJER2001), Science and Technology Platform Program for Advanced Biological Medicine JP21am0401011, AMED-CREST JP21gm0610006 (AMED/MEXT) (H.R.U.), a Brain/MINDS JP21dm0207049, Grant-in-Aid for Scientific Research (S) JP18H05270 (JSPS KAKENHI) (H.R.U.) a JSPS KAKENHI grant-in-aid for scientific research (c) (K.M., no. 20K06885), a grant-in-aid from the Human Frontier Science Program (H.R.U.), a JST (Moonshot R&D) (K.M., no. JPMJMS2023), a MEXT Quantum Leap Flagship Program (MEXT QLEAP) (H.R.U., no. JPMXS0120330644) and an intramural Grant-in-Aid from the RIKEN BDR (H.R.U.).

Author contributions

H.R.U., K.M. and F.A. designed the study. F.A. performed most of the biological experiments. F.A. designed the tissue clearing insert device. K.M. designed and constructed the customized light-sheet fluorescence microscope. K.M. developed the cell detection program. F.A. and K.Y. performed imaging and data analysis. F.A., K.M. and H.R.U. wrote the manuscript. All authors discussed the results and commented on the manuscript text.

Competing interests

H.R.U. has filed a patent (PCT/JP2014/070618, 2013-168705) application of the CUBIC protocol. H.R.U. and K.M. are sideworkers at CUBICStars Inc. and hold shares in the company.

Additional information

Supplementary information The online version contains supplementary material available at https://doi.org/10.1038/s41596-024-01080-1.

Correspondence and requests for materials should be addressed to Hiroki R. Ueda.

Peer review information *Nature Protocols* thanks Hans-Ulrich Dodt and Per Uhlen for their contribution to the peer review of this work.